

Supporting Information

Molecular Recognition between Bacterial Phosphorothioate DNA and Sulfur-Binding Protein SBD: Competition between Water Cage and Chalcogen-Hydrophobic Pocket

Jiayi Li, Haibo Wan, Haoqing Zhang, Xiao-Lei Wang, Guang Liu, * Geng Wu, Xinyi He, Zixin Deng, Yi-Lei Zhao*

State Key Laboratory of Microbial Metabolism, Joint International Research Laboratory of Metabolic and Developmental Sciences, School of Life Sciences and Biotechnology, Shanghai Jiao Tong University, Shanghai 200240, China

*To whom correspondence should be addressed: Prof. Yi-Lei Zhao Tel/Fax: +86-21-34207190; Email: yileizhao@sjtu.edu.cn or Dr. Guang Liu, email: jyayann@sjtu.edu.cn

Contents

Fig. S1: H-bonding angle distributions of the S_{P2} and O_{P2} atoms in water	S3
Fig. S2: H-bond numbers of the S_{P2} and O_{P2} atoms in water	S4
Fig. S3: Snapshots of H-bonds surrounding the S_{P2} atoms	S5
Fig. S4: Snapshots of H-bonds surrounding the O_{P2} atoms.....	S6
Fig. S5: DFT-optimized H-bond models of the S_{P2} and O_{P2} atoms	S7
Fig. S6: RMSD of 1.2 μ s MD trajectories for the <i>holo</i> -systems	S8
Fig. S7: Binding energy decomposition for individual residues	S9
Fig. S8: Orbital interaction diagram of the P165-PO complex	S10
Fig. S9: IGM analysis of SBD binding pocket	S11
Fig. S10: Electrostatic potential surfaces of the PS-P165 complex model.....	S12
Fig. S11: AIM analysis of the PS-P165 complex model	S13
Fig. S12: Curve fittings in the K_d -measuring experiments.....	S14
Fig. S13: Contact analysis of A117 variant in the PT-DNA SBD complex.....	S15
Fig. S14: Contact analysis of R168 variant in the PT-DNA SBD complex	S16
Fig. S15: Contact analysis of M164 variant in the PT-DNA SBD complex	S17
Fig. S16: Hydration analysis of DNA-SBD complex.....	S18
Fig. S17: Water numbers analysis around S_{P2}/O_{P2} atoms during the MD simulations	S19
Fig. S18: Conformational comparison of A168 mutants in PT-DNA SBD complex	S20
Fig. S19: Conformational comparison of A168 mutants in normal DNA SBD complex ..	S21
Table S1: K_d S of PS-ODN and target proteins reported in literature.....	S22
Table S2: Calculated $dV/d\lambda$ in the four TI cycles	S23-S26
Table S3: MMGBSA results for PT-DNA binding SBD variants.....	S27
Table S4: MMGBSA results for normal DNA binding SBD variants.....	S28
Table S5: Primers used for constructing SBD variants expression vectors.	S29
Table S6: Local structures of PT and protein complexes.....	S30-S34
Alchemical Binding Free Energy Calculation details	S35
MM/GBSA binding energy calculation details	S36
Non-covalent interaction analysis details.....	S37-S38
Geometries of the complexes in the QM calculation.....	S39-S41

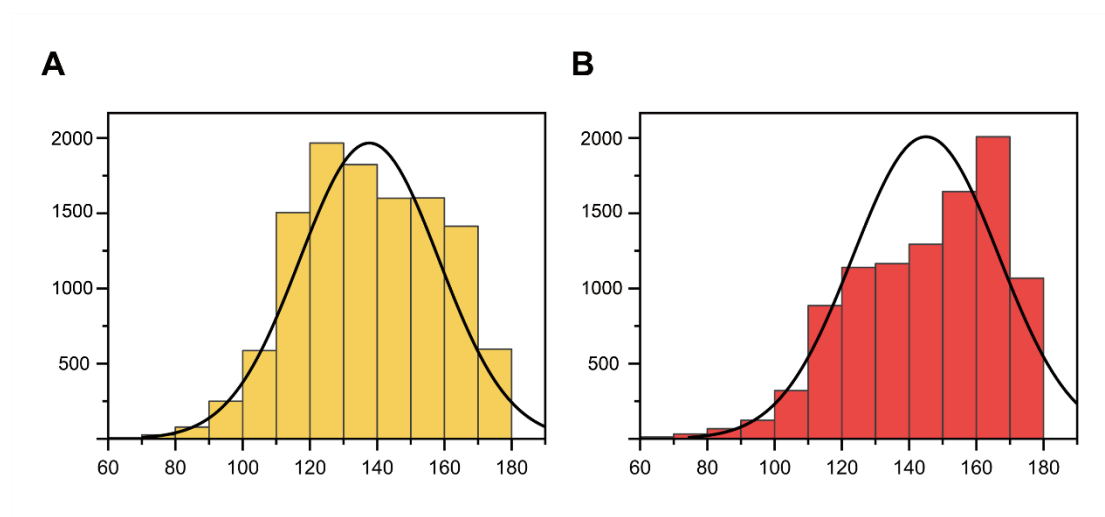


Fig. S1: H-bonding angle distributions of the S_{P2} and O_{P2} atoms of (A) apo-PT DNA and (B) apo-normal DNA in the water.

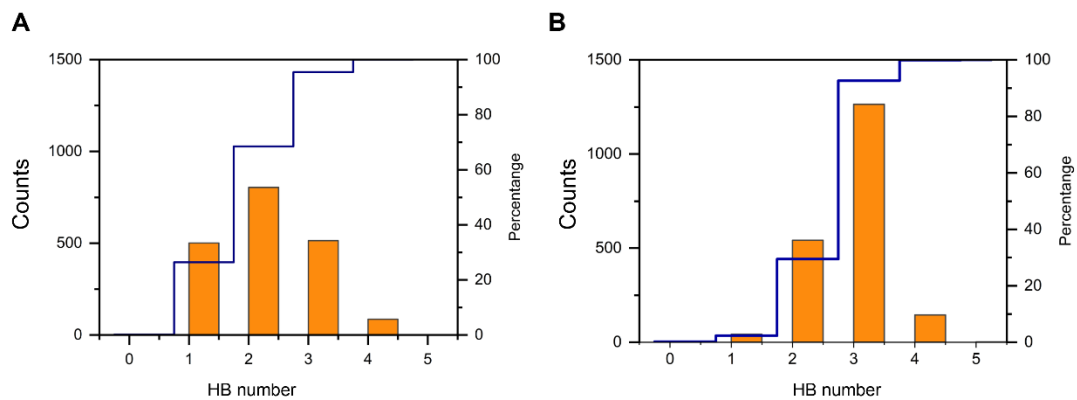


Fig. S2 H-bonding angle distributions of the S_{P2} and O_{P2} atoms in water. S_{P2} and O_{P2} atom was selected to represented the H-bonding angle differences of (A) *apo*-PT DNA and (B) *apo*-normal DNA during the MD simulations.

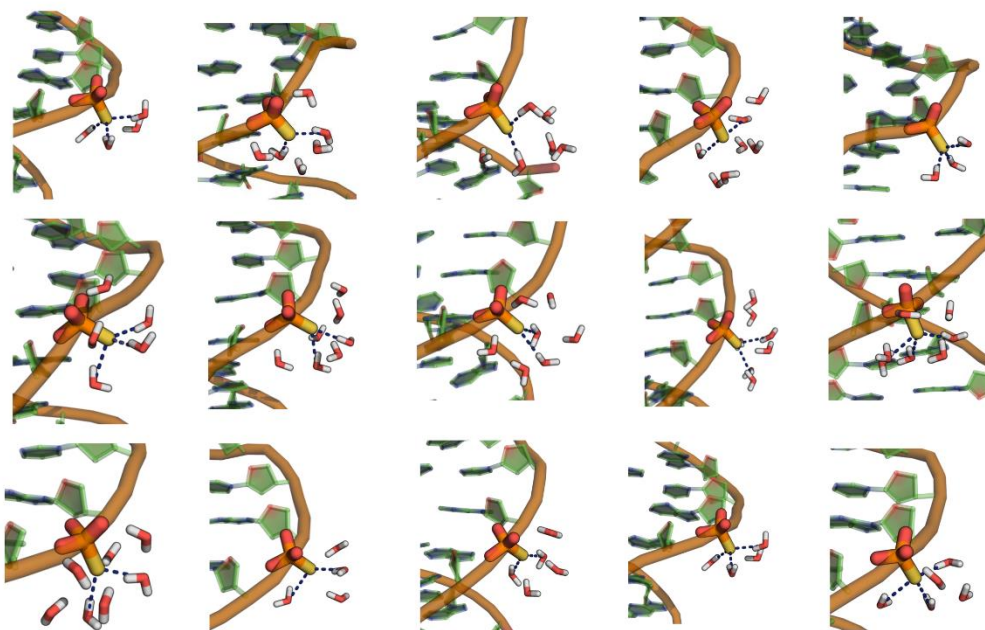


Fig. S3 Snapshots of H-bonds surrounding the S_{P2} atoms. The sites of phosphonothioate modification of *apo*-DNA during the MD simulations and the surrounding water molecules that form hydrogen bonds with S_{P2} atoms are highlighted.

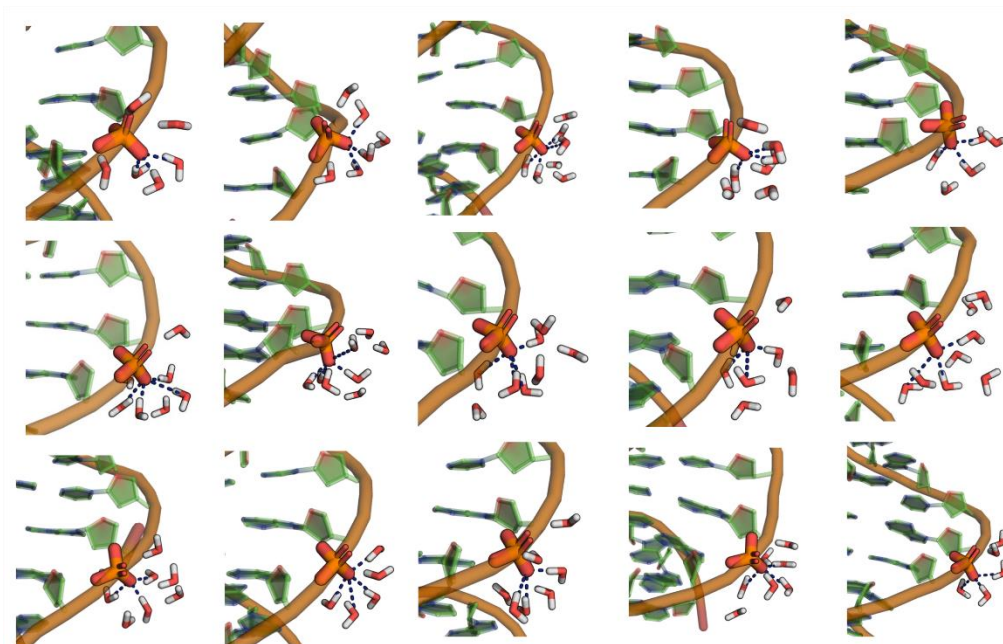


Fig. S4 Snapshots of H-bonds surrounding the O_{P_2} atoms. The sites of O_{P_2} atom of *apo*-normal DNA and the surrounding water molecules that forming hydrogen bonds are highlighted.

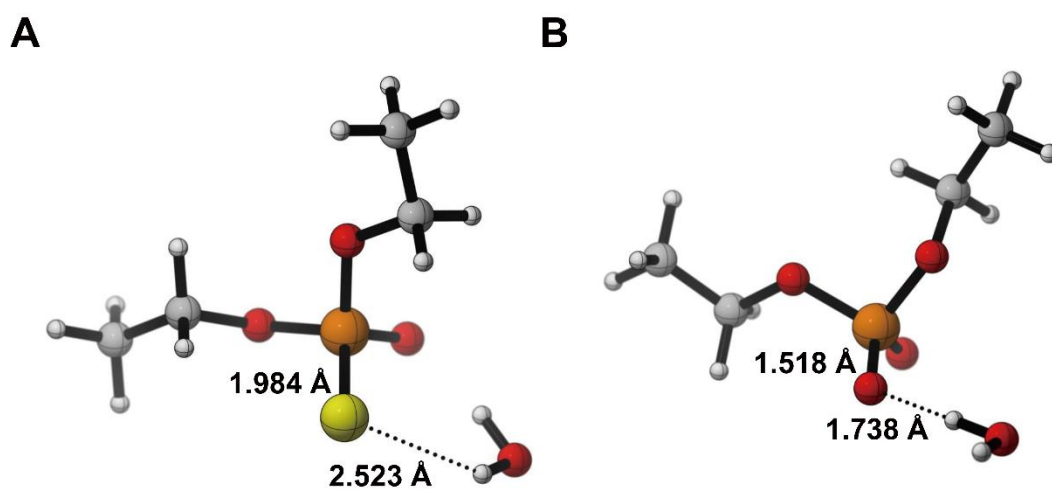


Fig. S5 DFT-optimized H-bond models of the S_{p2} and O_{p2} atoms. The (A) PS-H₂O model and (B) PO-H₂O model was optimized at B3LYP-D3(BJ)/Def2-TZVP/SMD (water) level of theory. For simplicity, diethyl thiophosphate ester (DETP) analogue was used to represent the PS.

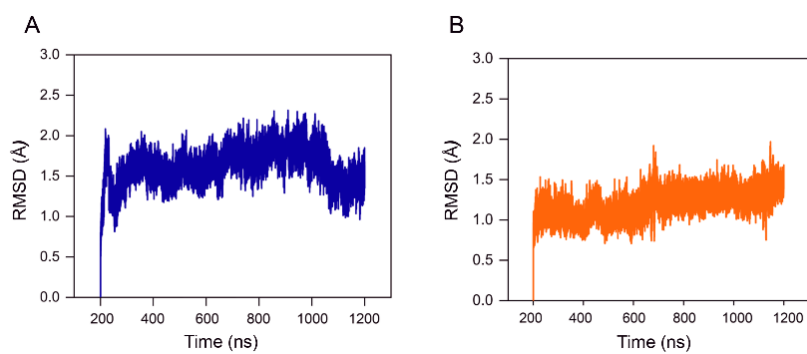


Fig. S6 RMSD of 1.2 μ s MD trajectories for the *holo*-systems. The alpha-carbon atoms of (A) *holo*-PT-DNA and (B) *holo*-normal DNA were superposed. Stable RMSD of the protein till the end of the simulation, suggested that the simulations were suitable for further rigorous analysis.

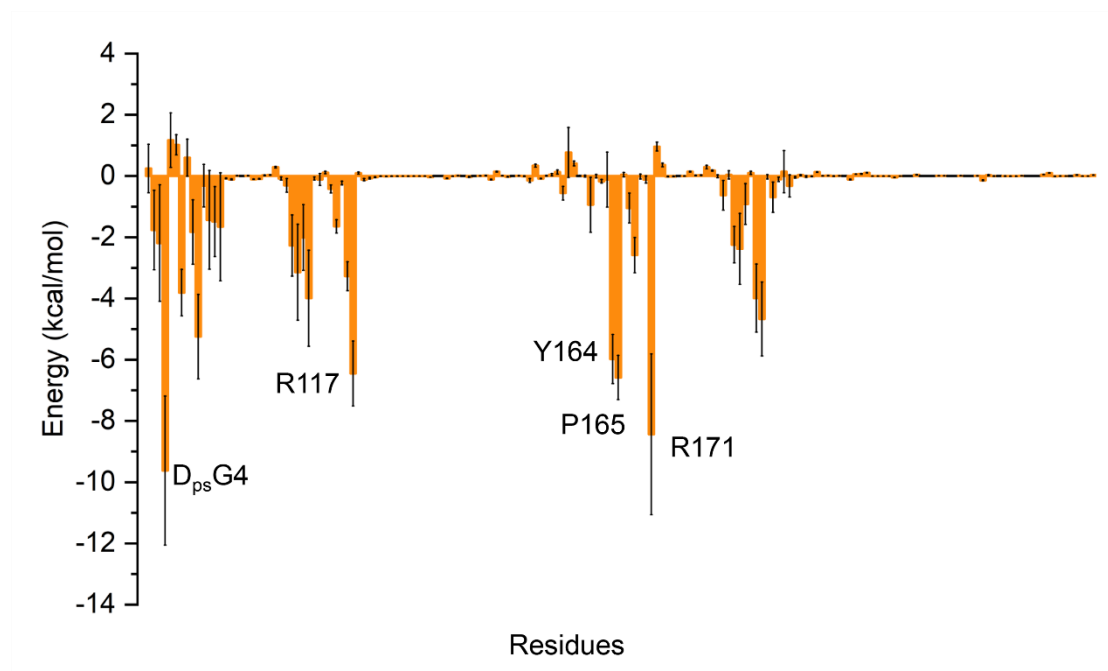


Fig. S7 Binding energy decomposition for individual residues. Residues contributions of *holo*-PT-DNA-SBD binding free energy (Unit=kcal/mol).

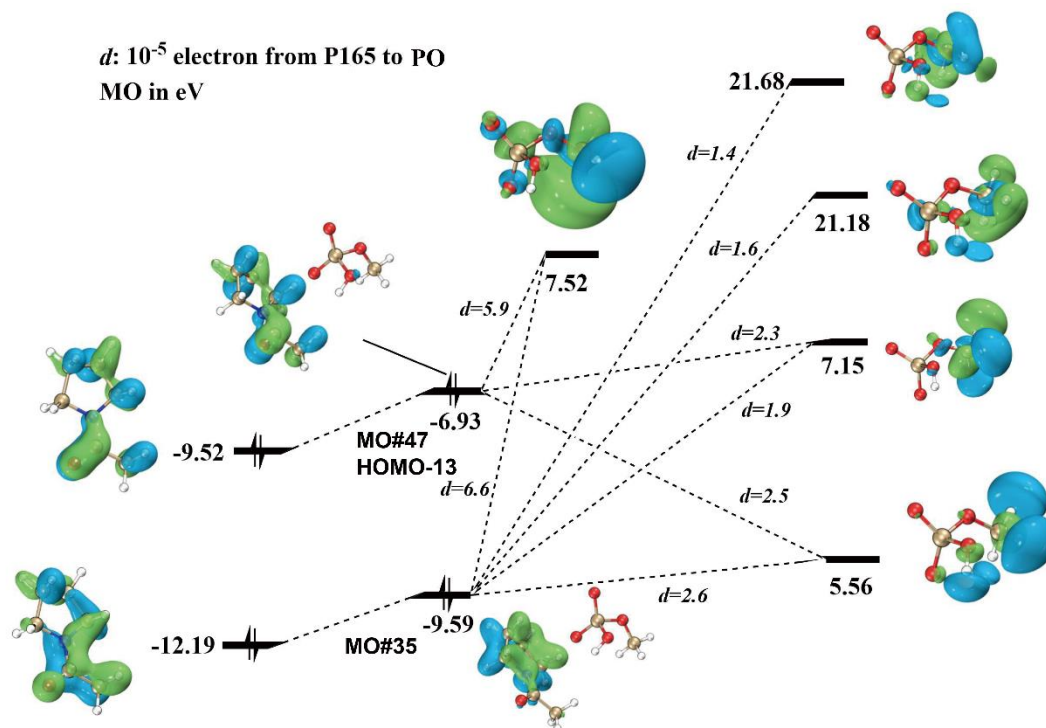


Fig. S8 Orbital interaction diagram of predicted electron delocalization from P165 to PO. Molecular orbitals (MO) of P165 (MO numbers 19, and 28), PO-P165 complex (MO numbers 35, and 47(HOMO-13)), and PO (MO numbers 30, 32, 33, 46 and 48) are shown.

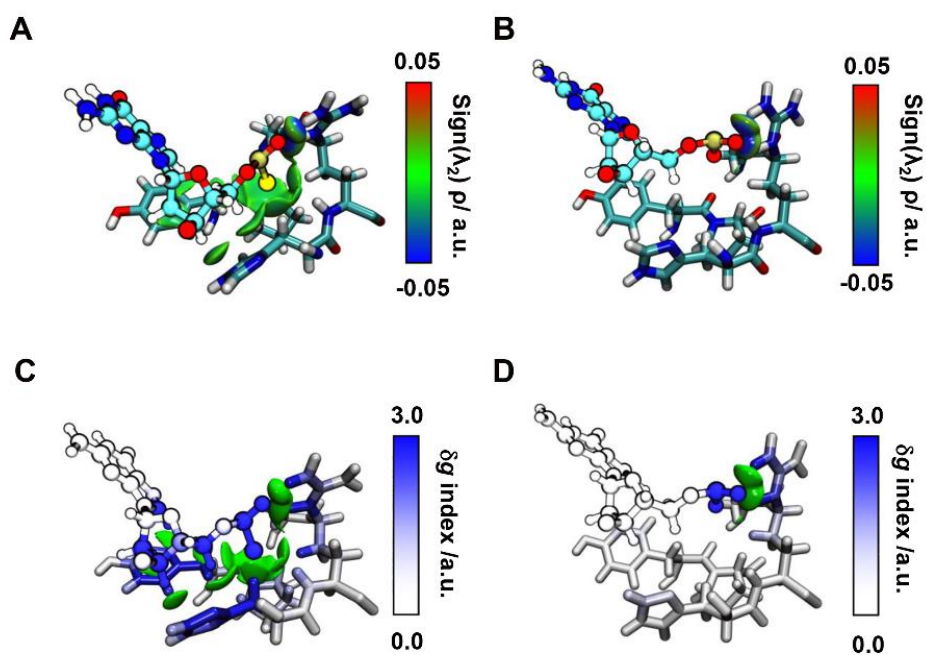


Fig. S9 Independent gradient model (IGM) analysis of binding pockets of PS/PO binding with SBD. $\delta g^{\text{inter}} = 0.05$ a.u. isosurfaces are colored by the sign of $(\lambda_2) \rho$ for binding pockets of (A) *holo*-PT-DNA and (B) *holo*-normal-DNA. *holo*-PT-DNA structure was obtained from the co-crystal structure (PDB ID:5ZMO). *holo*-normal-DNA structure was obtained from the average structure during the MD simulations. Blue color represented hydrogen bonding interaction, and green represented van der Waals interaction. All isosurfaces are colored according to a BGR (blue-green-red) scheme. Molecular structure coloring based on atom δg indices. The atoms of (C) PS and (D) PO are colored according to their contributions to the binding with SBD. White indicates no contribution to the complexation, and blue indicates the largest relative contribution.

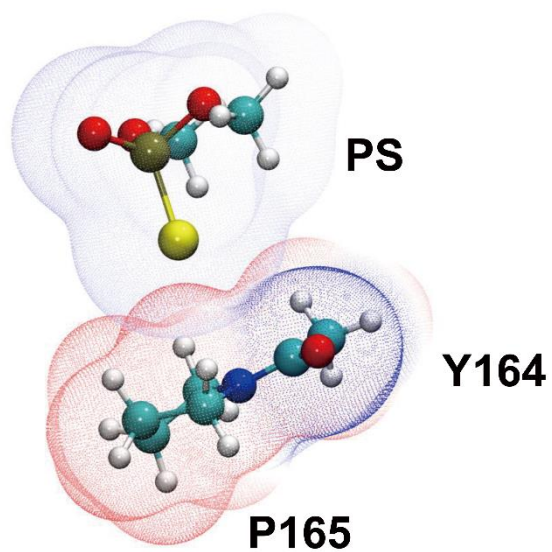


Fig. S10 Electrostatic potential surfaces of the PS-P165 complex model. The electrostatic potential surface (ESP) of PS-P165 calculation model was analyzed by Multiwfn package on isosurfaces of electronic density 0.003 a.u..

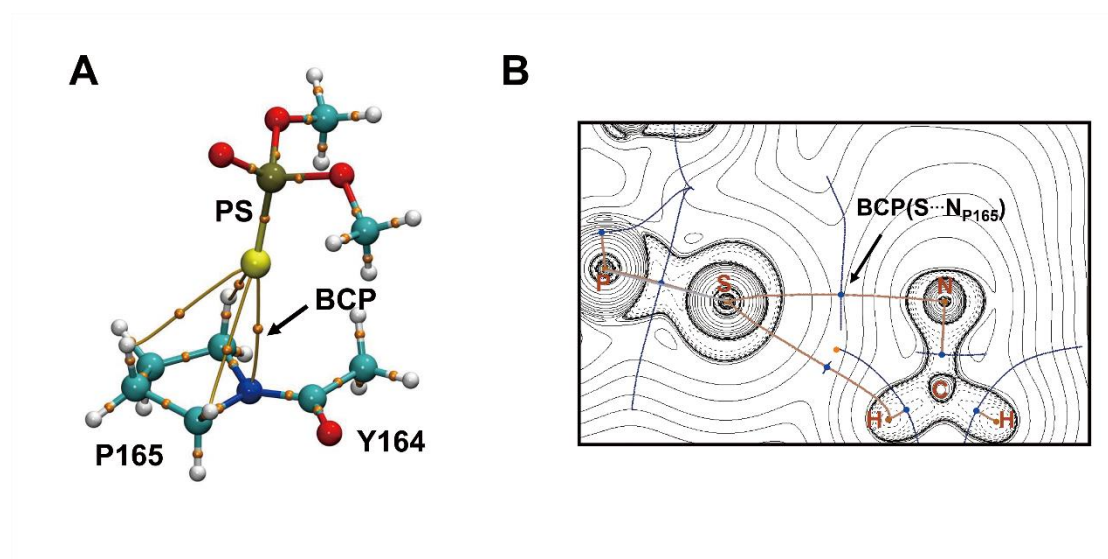


Fig. S11 AIM analysis of the PS-P165 complex model. (A) Bond critical points (BCPs) and bonding paths were obtained from the complex model. (B) Contour line diagram of the Laplacian distribution, $\nabla^2\rho(r)$, zero flux surfaces and bond paths were showed in the P-S...N_{P165} plane.

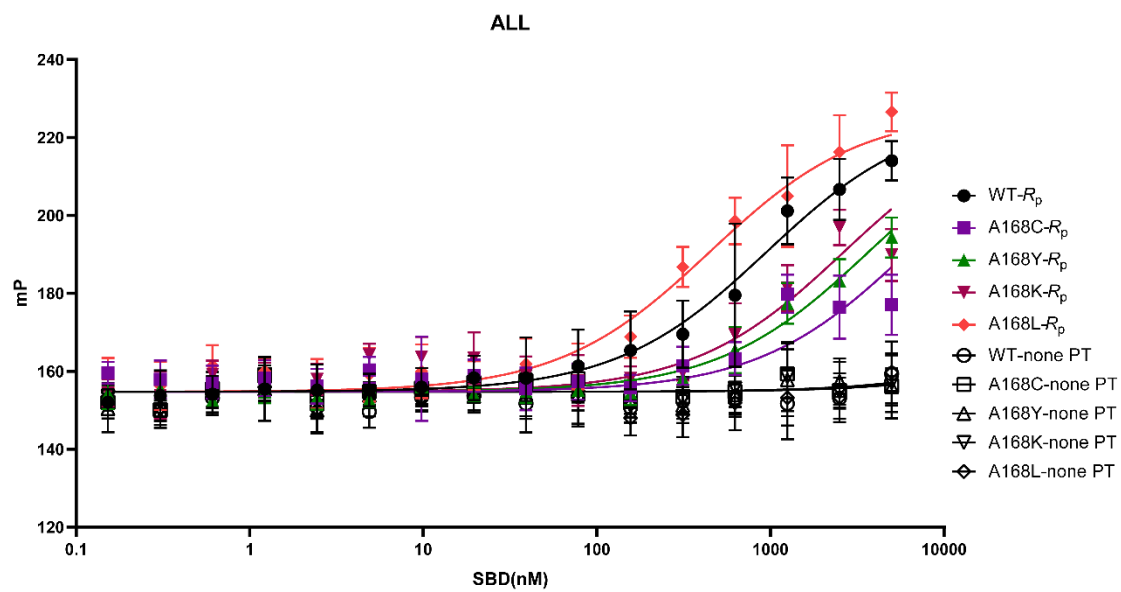


Fig. S12 Curve fittings in the K_d -measuring experiments. The dissociation constant of various point mutants of SBD binding with PT-DNA and normal DNA were measured via fluorescence polarization assay.

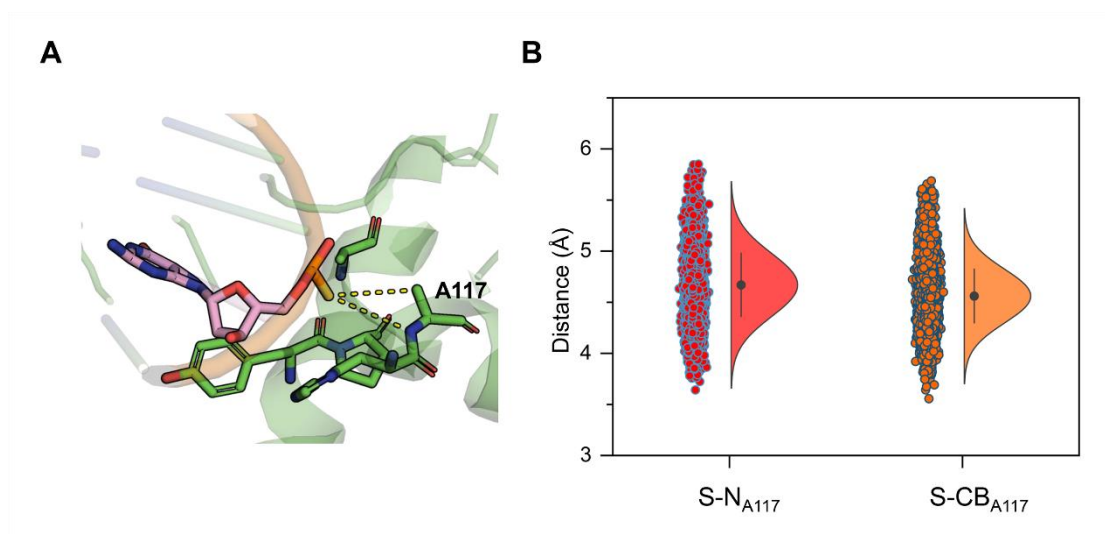


Fig. S13 Contact analysis of A117 variant in the PT-DNA SBD complex. (A) Representative MD frames of R117A in complex with PT-DNA. Non-covalent interaction was shown in yellow dash lines. (B) The frequency distribution of distance of S-CB_{A117} and S-N_{A117}. Distances are in Angstroms.

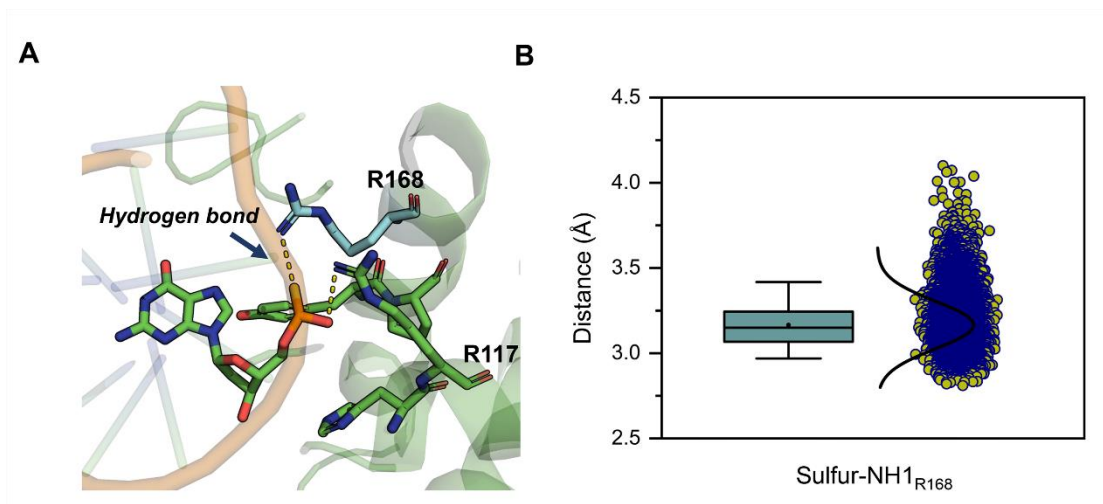


Fig. S14 Contact analysis of R168 variant in the PT-DNA SBD complex. (A) Representative snapshot of PT-DNA-A168R was obtained from the MD trajectories. (B) The frequency distribution of distances between S_{P2} atom and NH1 atom of R168. Distances are in Angstroms.

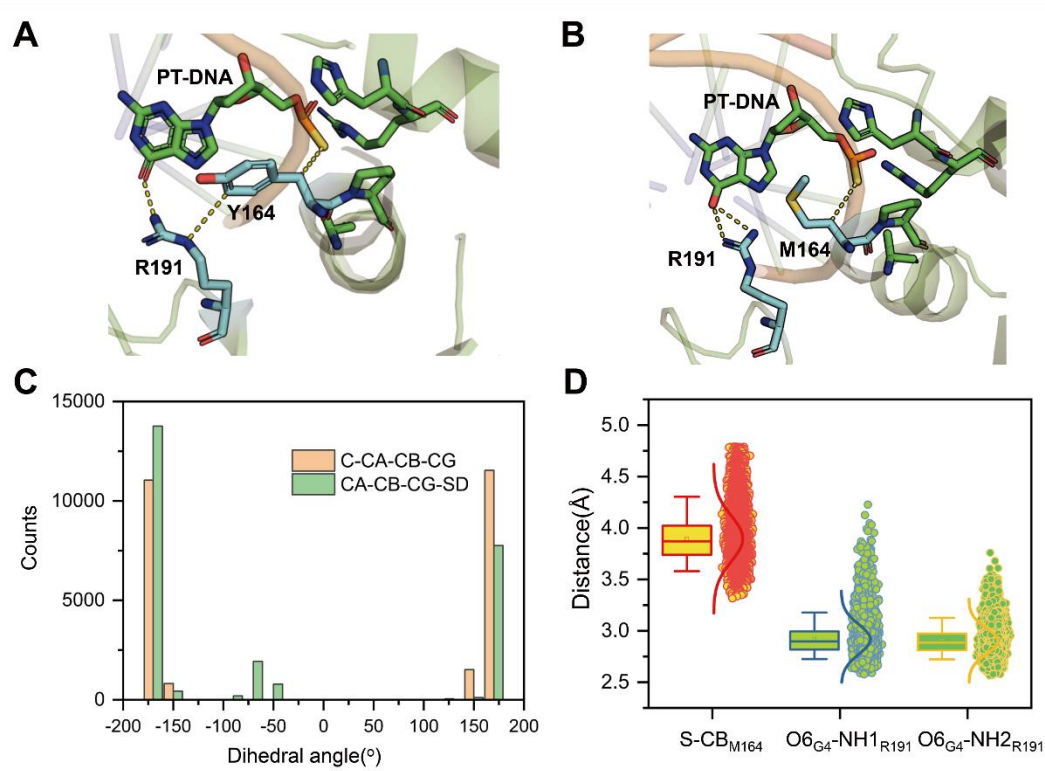


Fig. S15 Contact analysis of M164 variant in the PT-DNA SBD complex. (A) The co-crystal structure of PS-SBD (PDB ID:5ZMO). (B) A representative snapshot of PS-Y164M after clustering analysis during MD simulation. (C) The frequency distribution of dihedral of residue M164 during the MD simulations (D) Quantify the non-covalent interaction across simulations by measuring the distance of G4 base-M164 and G4 base-R19.

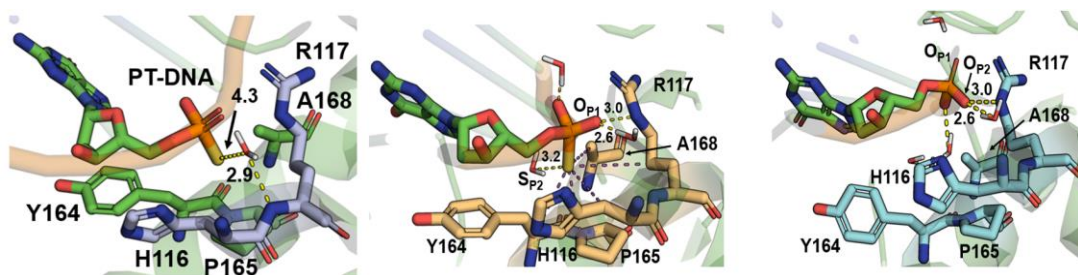


Fig. S16: Water molecules in the PT-DNA/SBD co-crystal structure (left), and the representative MD snapshots of the PT-DNA/SBD (middle) and normal DNA/SBD (right) complexes. (The representative frames selected with the cluster analysis, sulfur-recognizing residues in stick, and the heavy-atom distances marked with yellow dash lines and in angstroms.)

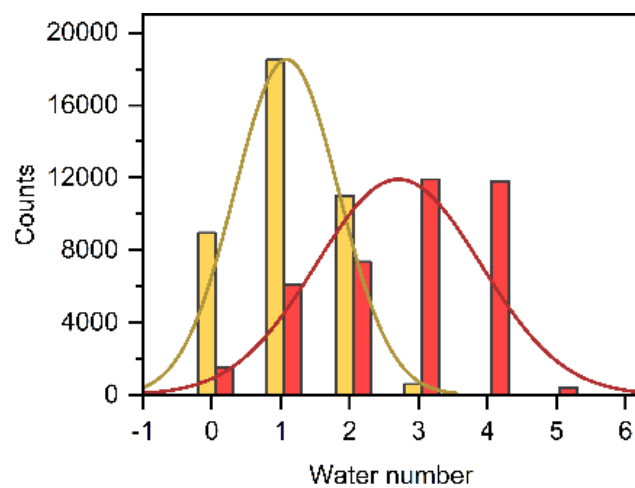


Fig. S17: Frequency distribution graph exhibited the water numbers in a range of 4 to 5 Å to the S_{p2} and O_{p2} atoms in the MD simulations of PT-DNA/SBD and normal DNA/SBD systems.

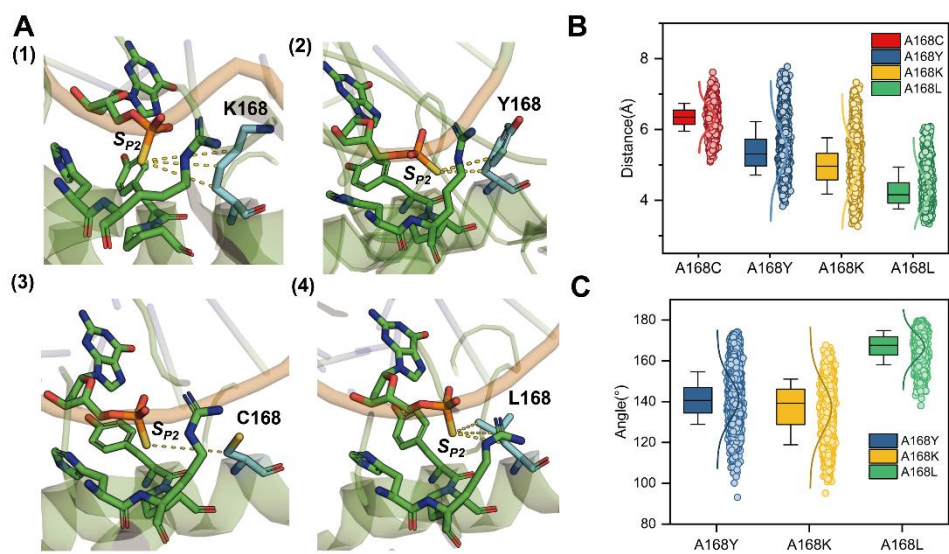


Fig. S18: Conformational comparison for the A168 mutants. (A) representative structures of variants (1) A168K, (2) A168Y, (3) A168C and (4) A168L, based on cluster analysis of the MD trajectories, (B) the distances between the S_{P2} atom and >C_βH₂ of the 168 sites, and (C) the ChB angle of P-S---N^{P165} in the MD simulation of PT-DNA/SBD systems.

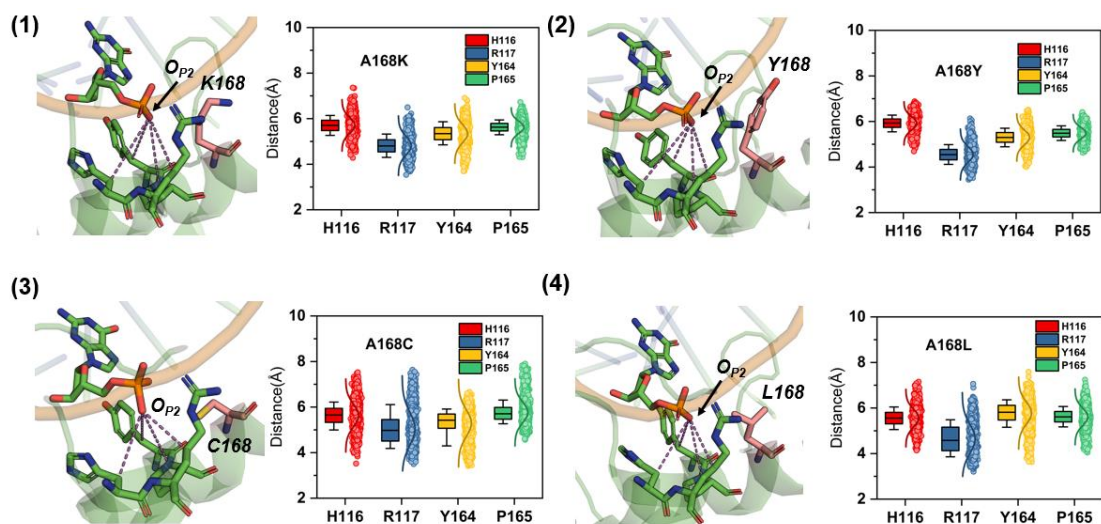


Fig. S19: Conformational comparison for the A168 mutants in normal DNA-SBD complexes. Representative structures of variants and the distance analysis of (1) A168K, (2) A168Y, (3) A168C and (4) A168L, based on cluster analysis of the MD trajectories. The frequency distribution counts the distance between the S_{P2} atom and C_{β}^{H116} , C_{β}^{Y164} , N^{P165} , C_{δ}^{R117} atoms.

Table S1 K_d s of PS-ODN and target proteins reported in literature. K_d value of PO and PS units binding with protein was reported, respectively. Environments of PO units for which replacement by PS triggers variable gains in binding affinity.

Kd	Kd	Binding affinity improvement	Year ^{ref}
PO2: 11 nM	PS2: 2.9 nM	4-fold	2015 ¹
PO2: 1.54 nM	PS2: 21.8 pM	70-fold	2017 ²
PO-DNA: 1.091e-007 M	PS-DNA: 9.725e-010 M	100-fold	2018 ³
PO-RNA: 6.361e-008 M	PS-RNA: 9.307e-010 M	60-fold	2018 ³
PO: 55.1±16 nM	PS: 0.7±0.2 nM	80-fold	2020 ⁴
PO2-RNA: 961.0±25.0 pM	PS2-RNA: 1.0±0.1 pM	1000-fold	2016 ⁵

Reference:

- Zandarashvili, L.; Nguyen, D.; Anderson, K. M.; White, M. A.; Gorenstein, D. G.; Iwahara, J. *Biophys. J.* 2015, **109**, 1026-1037
- Yang, X.; Abeydeera, N. D.; Liu, F.-W.; Egli, M. *Chem. Commun.* 2017, **53**, 10508
- W. Shen, C. L. De Hoyos, H. Sun, T. A. Vickers, X.-h. Liang and S. T. Crooke, *Nucleic Acids Res.*, 2018, **46**, 2204-2217.
- Hyjek-Skladanowska, M.; Vickers, T. A.; Napiorkowska, A.; Anderson, B. A.; Tanowitz, M.; Crooke, S. T.; Liang, X. H.; Seth, P. P.; Nowotny, M. *J. Am. Chem. Soc.* 2020, **142** (16), 7456-7468.
- N. D. Abeydeera, M. Egli, N. Cox, K. Mercier, J. N. Conde, P. S. Pallan, D. M. Mizurini, M. Sierant, F. E. Hibti, T. Hassell, T. Wang, F. W. Liu, H. M. Liu, C. Martinez, A. K. Sood, T. P. Lybrand, C. Frydman, R. Q. Monteiro, R. H. Gomer, B. Nawrot and X. Yang, *Nucleic Acids Res.*, 2016, **44**, 8052–8064.

Table S2 Calculated $dV/d\lambda$ in the four TI cycles. Calculated $dV/d\lambda$ values and errors (deviation) of the eight curves in four different thermodynamic cycle in thermodynamic integration (TI) calculation.

Thermodynamic cycle1: Cycle1 estimates the mutation effect from ds-modified-PT-DNA to hemi-modified (DSG10)-PT-DNA on binding with SBD

Lambda	ds-modified-PT-DNA	Standard deviation	hemi-modified (DSG10)-PT-DNA-SBD	Standard deviation
0	9.9±0.2	4.7	24.7±0.2	6.3
0.01	8.8±0.1	4.4	24.7±0.2	6.3
0.02	8.2±0.1	4.2	21.4±0.2	6.1
0.03	7.9±0.2	4.6	19.2±0.2	6.3
0.04	7.7±0.2	4.5	19.3±0.2	5.7
0.05	5.6±0.2	4.9	17.8±0.1	5.5
0.10	5.8±0.2	3.6	13.1±0.1	5.4
0.15	4.5±0.2	3.5	8.1±0.1	5.3
0.20	2.2±0.2	3.9	5.9±0.1	4.8
0.25	2.1±0.1	3.5	3.8±0.1	4.7
0.30	0.5±0.1	3.7	-0.6±0.1	5.3
0.35	-0.5±0.1	3.2	-2.1±0.1	5.1
0.40	-0.7±0.1	2.9	-4.9±0.1	5.2
0.45	-0.8±0.1	2.9	-9.9±0.2	6.6
0.50	-1.9±0.1	2.7	-8.5±0.1	5.3
0.55	-2.0±0.1	2.5	-10.1±0.2	4.4
0.60	-3.1±0.1	2.5	-11.8±0.2	4.0
0.65	-4.5±0.1	3.1	-14.6±0.2	4.2
0.70	-5.6±0.1	2.3	-16.3±0.1	4.3
0.75	-5.4±0.1	2.3	-16.9±0.1	4.7
0.80	-4.9±0.1	1.7	-22.7±0.2	6.0
0.85	-6.9±0.1	3.3	-33.0±0.2	7.9
0.90	-8.5±0.1	2.7	-46.6±0.2	9.1
0.95	-10.1±0.3	3.7	-64.3±0.2	12.8
0.96	-12.3±0.1	3.4	-76.9±0.2	12.8
0.97	-17.5±0.1	5.4	-83.9±0.2	13.9
0.98	-19.8±0.4	4.1	-86.4±0.3	15.4
0.99	-24.4±0.6	5.5	-98.9±0.3	16.4
1.00	-35.4±0.9	9.3	-115.1±0.4	18.2

Thermodynamic cycle2: cycle2 estimates the mutation effect from hemi-modified (DSG10)-PT DNA to normal DNA on binding with SBD

Lambda	hemi-modified (DSG10)-PT DNA-SBD	Standard deviation	hemi-modified (DSG10)-PT DNA	Standard deviation
0	29.6±0.2	6.5	24.7±0.2	6.3
0.01	29.2±0.2	5.7	24.7±0.2	6.3
0.02	26.4±0.2	5.7	21.4±0.2	6.1
0.03	25.4±0.2	5.5	19.2±0.2	6.3
0.04	23.7±0.2	5.3	19.3±0.2	5.8
0.05	22.2±0.2	5.1	17.8±0.2	5.5
0.10	16.4±0.2	4.7	13.1±0.2	5.4
0.15	12.4±0.2	4.4	8.1±0.2	5.3
0.20	8.2±0.2	4.5	5.9±0.2	4.8
0.25	4.7±0.2	4.5	3.8±0.2	4.7
0.30	2.0±0.2	4.5	-0.6±0.2	5.3
0.35	-0.7±0.2	4.7	-2.1±0.2	5.1
0.40	-3.2±0.2	4.9	-4.9±0.2	5.2
0.45	-6.5±0.2	5.5	-9.9±0.2	6.6
0.50	-10.1±0.2	5.6	-8.5±0.2	5.3
0.55	-12.3±0.2	5.3	-10.1±0.1	4.4
0.60	-14.9±0.2	4.7	-11.9±0.2	4.0
0.65	-17.1±0.2	4.3	-14.6±0.1	4.2
0.70	-19.8±0.2	4.4	-16.3±0.2	4.3
0.75	-24.1±0.2	4.7	-17.0±0.2	4.7
0.80	-29.8±0.2	5.5	-22.7±0.2	6.0
0.85	-38.2±0.2	6.2	-32.9±0.3	7.9
0.90	-47.9±0.3	10.4	-46.6±0.3	9.1
0.95	-72.9±0.4	11.1	-64.3±0.4	12.8
0.96	-80.1±0.4	12.4	-77.0±0.4	12.8
0.97	-87.9±0.4	13.6	-83.9±0.2	13.9
0.98	-95.4±0.5	14.1	-86.4±0.2	15.4
0.99	-104.5±0.5	15.6	-99.0±0.5	16.4
1.00	-117.1±0.6	17.9	-115.1±0.6	18.2

Thermodynamic cycle3: cycle3 estimates the mutation effect from ds-modified-PT-DNA to hemi-modified (DSG4)-PT-DNA on binding with SBD

Lambda	ds-modified-PT-DNA	Standard deviation	ds-modified-PT-DNA-SBD	Standard deviation
0	24.1±0.2	6.5	24.6±0.2	6.6
0.01	23.4±0.2	6.2	22.4±0.2	6.5
0.02	19.8±0.2	6.6	22.9±0.2	6.3
0.03	20.4±0.2	6.2	20.3±0.2	5.5
0.04	19.5±0.2	5.8	17.9±0.2	6.0
0.05	17.5±0.2	5.9	17.6±0.2	5.6
0.10	12.4±0.2	5.7	12.5±0.2	5.8
0.15	7.7±0.2	5.4	8.3±0.2	5.3
0.20	4.9±0.2	5.3	4.4±0.2	5.5
0.25	3.4±0.2	5.1	1.1±0.2	5.8
0.30	-2.7±0.2	6.5	-0.1±0.2	5.2
0.35	-3.3±0.2	5.2	-1.5±0.2	4.6
0.40	-4.6±0.2	4.9	-3.8±0.2	4.6
0.45	-9.8±0.2	6.3	-7.1±0.2	5.1
0.50	-9.9±0.2	5.6	-10.1±0.2	5.6
0.55	-10.8±0.2	4.8	-11.8±0.2	5.3
0.60	-12.8±0.2	3.9	-12.2±0.2	4.2
0.65	-13.5±0.2	3.9	-13.2±0.2	3.9
0.70	-14.7±0.2	4.1	-14.5±0.2	4.6
0.75	-18.9±0.2	5.0	-17.8±0.2	5.2
0.80	-24.1±0.2	5.8	-22.1±0.2	6.2
0.85	-32.1±0.2	8.1	-29.6±0.2	7.5
0.90	-46.1±0.3	9.2	-47.7±0.3	9.5
0.95	-67.4±0.4	12.9	-69.8±0.4	12.5
0.96	-72.8±0.5	13.8	-75.5±0.5	14.0
0.97	-79.9±0.5	15.1	-83.5±0.5	14.8
0.98	-89.9±0.5	15.9	-89.5±0.5	14.9
0.99	-100.7±0.6	16.9	-106.9±0.5	16.3
1.00	-111.0±0.6	18.5	-112.7±0.6	17.8

Thermodynamic cycle4: cycle4 estimates the mutation effect from hemi-modified (DSG4)-PT-DNA to normal DNA on binding with SBD.

Lambda	Free-protein	Standard deviation	Free-protein	Standard deviation
0	9.9±0.1	4.3	27.9±0.2	5.9
0.01	8.7±0.1	4.8	25.6±0.2	6.2
0.02	9.4±0.1	4.2	23.9±0.2	5.8
0.03	9.0±0.1	4.2	22.4±0.2	5.8
0.04	9.6±0.1	3.7	22.2±0.2	5.5
0.05	7.99±0.1	3.8	20.6±0.2	5.4
0.10	6.1±0.1	3.6	14.8±0.2	5.0
0.15	5.3±0.1	3.1	10.7±0.2	4.4
0.20	4.8±0.1	3.0	7.0±0.1	4.5
0.25	2.8±0.1	3.3	4.2±0.2	4.2
0.30	1.9±0.1	2.9	0.9±0.2	4.3
0.35	0.9±0.1	3.0	-1.9±0.2	5.3
0.40	0.5±0.1	2.5	-3.7±0.2	4.7
0.45	-1.5±0.1	3.2	-3.0±0.2	7.1
0.50	-1.3±0.1	2.5	-9.3±0.2	5.2
0.55	-4.5±0.1	3.6	-12.6±0.2	5.7
0.60	-3.2±0.1	2.4	-15.3±0.2	4.7
0.65	-3.5±0.1	2.0	-17.8±0.2	4.2
0.70	-5.4±0.1	3.2	-20.2±0.5	4.6
0.75	-5.4±0.1	1.9	-23.5±0.2	4.8
0.80	-5.5±0.1	1.7	-30.0±0.6	5.6
0.85	-6.6±0.1	2.1	-38.1±0.2	6.5
0.90	-8.9±0.1	1.9	-51.1±0.3	8.4
0.95	-9.7±0.1	2.9	-73.9±0.4	11.5
0.96	-12.0±0.1	5.8	-75.1±0.5	14.5
0.97	-16.1±0.1	9.5	-84.7±0.5	14.5
0.98	-18.9±0.1	10.5	-95.4±0.5	15.1
0.99	-19.2±0.1	15.1	-105.4±0.5	15.1
1.00	-21.7±0.1	16.1	-114.7±0.6	17.0

Table S3 MMGBSA results for PT-DNA binding SBD variants. All energies in kcal/mol.

System	ΔE_{vdw}	ΔE_{ele}	ΔG_{GB}	ΔG_{SA}	ΔG_{bind}	$\Delta\Delta G_{\text{bind}}$
PT-DNA- WT-SBD	-75.2 ± 7.4	-1207.7 ± 79.8	1212.5 ± 76.6	-11.1 ± 0.8	-81.5 ± 8.2	0
PT-DNA- H116I	-87.2 ± 6.6	-1224.6 ± 102.0	1243.8 ± 95.1	-11.7 ± 0.8	-79.7 ± 12.7	3.9 ± 4.5
PT-DNA- R117K	-100.45 ± 8.16	-1306.84 ± 69.70	-1338.97 ± 65.48	-13.59 ± 1.01	-81.9 ± 9.1	-0.4 ± 1.7
PT-DNA- R117A	-87.9 ± 4.6	-758.7 ± 50.4	-799.2 ± 49.1	-11.3 ± 0.5	-58.8 ± 6.3	23.2 ± 1.8
PT-DNA- Y164M	101.6 ± 5.6	-1474.2 ± 78.1	1493.2 ± 74.4	-13.0 ± 0.5	-94.2 ± 8.3	-12.7 ± 0.1
PT-DNA- A168H	-80.3 ± 5.0	-1233.6 ± 59.5	1246.7 ± 52.8	-11.5 ± 0.4	-77.6 ± 10.0	3.9 ± 1.8
PT-DNA- A168R	-93.4 ± 5.6	-1262.3 ± 47.7	1280.7 ± 47.1	-12.4 ± 0.6	-87.5 ± 5.7	-5.9 ± 5.1
PT-DNA- A168C	-69.9 ± 5.8	-1348.0 ± 59.0	-1359.2 ± 54.6	-10.7 ± 0.6	-69.5 ± 8.3	12.0 ± 0.1
PT-DNA- A168Y	-83.1 ± 5.6	-1097.7 ± 53.9	-1118.5 ± 50.7	-11.0 ± 0.5	-73.3 ± 7.7	8.2 ± 0.5
PT-DNA- A168K	-72.7 ± 6.6	-1339.5 ± 79.1	1348.0 ± 69.4	-10.2 ± 0.7	-74.5 ± 8.9	7.0 ± 0.7
PT-DNA- A168L	-81.0 ± 7.6	-1450.8 ± 75.9	1456.6 ± 73.1	-11.6 ± 0.9	-86.8 ± 8.7	-5.3 ± 0.5

Note: $\Delta\Delta G_{\text{bind}} = \Delta G(\text{PS-Wt-SBD}) - \Delta G(\text{PS-Mutant-SBD})$

Table S4 MMGBSA results for normal DNA binding SBD variants. All energies in kcal/mol.

System	ΔE_{vdw}	ΔE_{ele}	ΔG_{GB}	ΔG_{SA}	ΔG_{bind}	$\Delta\Delta G_{\text{Calc}}$
PO-SBD	-75.2	-1119.9	1143.1	-10.8	-62.7	-18.8
	± 5.9	± 67.6	± 64.4	± 0.7	± 7.3	± 1.1
PO-A168C	-82.9	-836.3	869.7	-11.6	-61.2	-8.3
	± 8.6	± 75.9	± 73.5	± 1.2	± 10.3	± 2.0
PO-A168Y	-80.4	-1106.7	-1137.1	-11.2	-61.3	-12.0
	± 5.2	± 53.5	± 51.6	± 0.4	± 6.1	± 1.6
PO-A168K	-72.1	-1065.4	1088.2	-10.0	-59.3	-15.1
	± 7.3	± 79.7	± 73.2	± 0.7	± 9.6	± 1.3
PO-A168L	-77.8	-1117.1	1138.9	-11.3	-67.3	-19.5
	± 9.7	± 64.0	± 62.4	± 1.0	± 12.0	± 2.3

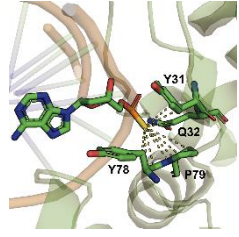
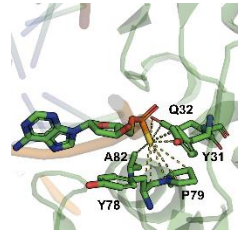
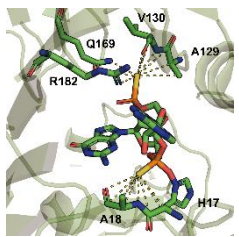
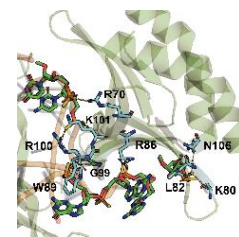
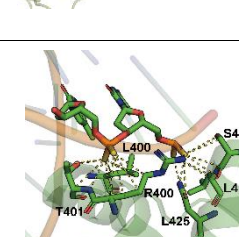
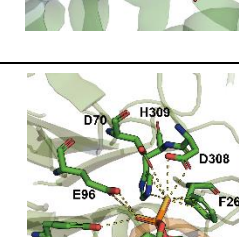
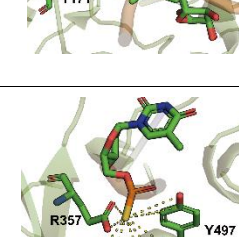
Note: $\Delta\Delta G_{\text{Calc}} = \Delta G(\text{PS-Protein}) - \Delta G(\text{PO-Protein})$. $\Delta G(\text{PS-Protein})$ can be found in Table S4, representing the binding energy calculated for PT-DNA in complex with wild type SBD and different mutants of A168C, A168Y, A168K, and A168L, respectively.

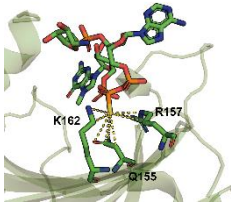
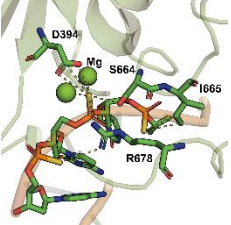
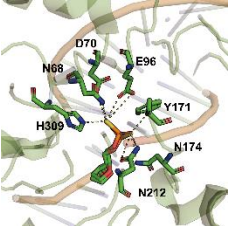
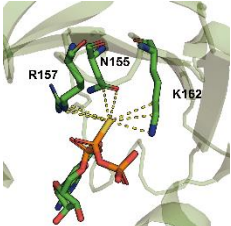
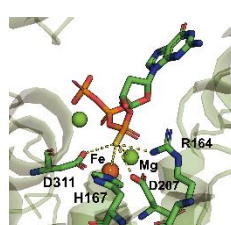
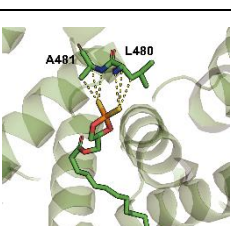
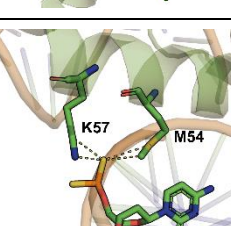
Table S5 Primers used for constructing SBD variants expression vectors

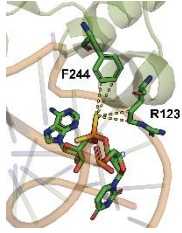
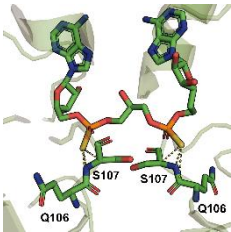
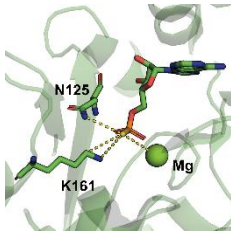
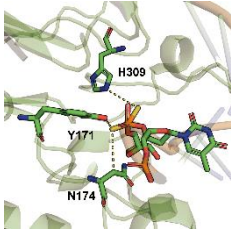
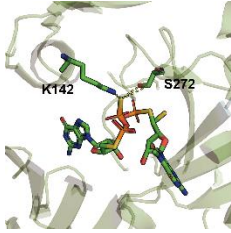
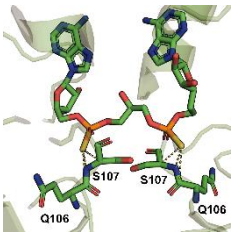
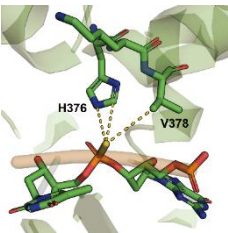
PRIMERS	SEQUENCE
A168C-F	ACCCATTCTGGTGCCTCGTGCGCGA
A168C-R	TCGCGCACGAGGCACCAGAATGGGT
A168Y-F	ACCCATTCTGGTACCTCGTGCGCGA
A168Y-R	TCGCGCACGAGGTACCAGAATGGGT
A168K-F	TCGCGCACGAGGTACCAGAATGGGT
A168K-R	TCGCGCACGAGCTTCCAGAATGGGT
A168L-F	ACCCATTCTGGCTCCTCGTGCGCGA
A168L-R	TCGCGCACGAGGAGCCAGAATGGGT
PT-GGCC-10-S	CCCG _{PS} GCCGCC
PT-GGCC-10-A	GGCGGCCGGG

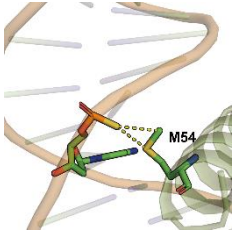
Table S6 Local structures of PT and protein complexes. A detailed description of the non-covalent interaction network surrounding sulfur atom about phosphorothioate-modified structure is reported in Table2. Several high contact numbers are observed. Usually, the high contact numbers suggest these artificial phosphorothioate nucleotides are good inhibitors for these functional proteins. In detail, the S2 atom of 6EA8 interacted with A129, V130, the side chain of Q169, and the guanidinium group of R182. In 6LFF, the S1 atom formed an electrostatic and hydrophobic interaction with R400, N425, and S421; the S2 atom developed close intercommunication with R400, T401, and L404. The S2 atom of 7LPI formed contacts with carboxylate groups of D308 and D70, as well as aromatic rings of H309 and F266. The S2 atom of 1KSP interacted with side chains of D355, E357, and E501 as well as the aromatic ring of Y497. The S2 atom of 6GKL formed the salt-bridge with positively charged side chains of R157 and K162 together with the polar side chain ($-\text{CH}_2-\text{CONH}$) of Q155. The S1 atom of 7LYT established positively charged side chains with D394, R678, and S664 along with two cofactor magnesium atoms. The S1 atom of 6GKK developed electrostatic interactions with NZ_{K162} (3.3Å) and NE_{R157} (3.6Å); methylene groups from Q155, R157, and K162 also provide additional vdW interactions. The S1 atom of 7A5Y had an electrostatic interaction with the side chains of H167, D207, R164, and D311, in addition to cofactor Fe and Mg atom.

PS/PS2 surrounding residues	PDB ID	Resolution	Local Environment of PS/PS2 surrounding residues
H116,R117,Y164, P165,A168	5ZMO	1.69 Å	
T31, Q32, Y78, P79 A82	7CC9	2.06 Å	

T31, Q32, Y78, P79	7CCJ	3.30 Å	
T31, Q32, Y78, P79 A82	7CCD	2.42 Å	
H17, A18, A129, V130, Q169, R182	6EA8	2.60 Å	
R70, K80, R86, W89, G99, R100, K101, N106	6YCS	3.05 Å	
R400, T401, L404, S421, L422, N425	6LFF	1.79 Å	
D70, E96, Y171, F266, D308, H309	7LPI	2.05 Å	
D355, E357, Y497, D501	1KSP	2.30 Å	

Q155, R157, K162	6GKL	2.20 Å	
D394, S664, I665 R678, Mg	7LYT	2.90 Å	
N68, D70, E96, Y171, N174, N212, H309	5DFI	1.63 Å	
N155, R157, K162	6GKK	1.86 Å	
Fe, Mg, R164, H167, D207, D311	7A5Y	2.29 Å	
L480 A481	5ID9	2.48 Å	
M54 K57	4XIC	2.69 Å	

R123 F244	5DO4	1.86 Å	 Molecular structure showing residues R123 and F244 in green stick representation, with dashed lines indicating interactions. The protein backbone is shown as a light green surface.
Q106, S107	4ZKL	2.34 Å	 Molecular structure showing residues Q106 and S107 in green stick representation, with dashed lines indicating interactions. The protein backbone is shown as a light green surface.
N125, K161, Mg	3OCZ	1.35 Å	 Molecular structure showing residues N125 and K161 in green stick representation, with a magnesium atom (Mg) shown as a green sphere. Dashed lines indicate interactions. The protein backbone is shown as a light green surface.
Y171, N174, H309	6W4T	2.77 Å	 Molecular structure showing residues Y171, N174, and H309 in green stick representation, with dashed lines indicating interactions. The protein backbone is shown as a light green surface.
K142 S272	5OSY	2.06 Å	 Molecular structure showing residues K142 and S272 in green stick representation, with dashed lines indicating interactions. The protein backbone is shown as a light green surface.
Q106, S107	4ZKL	2.34 Å	 Molecular structure showing residues Q106 and S107 in green stick representation, with dashed lines indicating interactions. The protein backbone is shown as a light green surface.
H376, V378	6U6Z	2.10 Å	 Molecular structure showing residues H376 and V378 in green stick representation, with dashed lines indicating interactions. The protein backbone is shown as a light green surface.

M54	5JLW	2.09 Å	
-----	------	--------	--

SUPPLEMENTARY METHOD

Alchemical Binding Free Energy Calculation details

In this study, we performed alchemical transformations of PT-DNA into normal DNA via sulfur-oxygen swap. To assess the change in the binding free energy between two different DNA in the SBD, thermodynamic integration (TI) performed relative free energy calculations. The free energy differences between PT-DNA and normal DNA were calculated by gradually perturbing from one to another in a series of discrete steps, represented by λ values. A series of artificial states, parametrized by λ , connecting the unmodified and modified forms, were created by interpolating the force field parameters. We used the notation that $\lambda = 0$ corresponds to unmodified states (normal DNA) and $\lambda = 1$ corresponds to modified states (PT-DNA). The free energy changes between adjacent states were estimated by the Bennett acceptance ratio (BAR) method (2). In this TI calculation, from 0.05 to 0.95, the interval of λ is 0.05. In the range of 0 to 0.05 and 0.95 to 1, to ensure the convergence and accuracy of the calculation, the interval of λ is chosen to be 0.01. In total, 29 λ -windows for each DNA transformation were performed. At each λ window, we carried out 500 steps of steepest descent minimization, a 50 ps density equilibration run, and a 2 ns NPT production run. The conformation of the mutant residue was taken from the most populated conformation sampled during standard MD simulations. A time step of 1 fs is used together with the SHAKE. TI calculations in water were performed with explicit solvent (TIP3P, minimum 12 Å to the box side) and under periodic boundary conditions with PME.

The conformation of the *holo*-PT-DNA was taken from the most populated conformation sampled during standard MD simulation. To improve convergence, “soft-core” potentials were applied both to the Lennard-Jones and the Coulombic potentials as implemented in AMBER 18. This makes it possible to perform both charge and van der Waals mutations in the same step, and therefore, the alchemical transformation was carried out in a single step, referred to as the single-transformation approach (STA). Free energy derivatives ($\partial V/\partial\lambda$) were collected independently for each λ from the production run. In the TI method, the free energy difference is calculated from the integral of $\partial V(\lambda)/\partial\lambda$ from 0 to 1, where V is the potential energy.

MM/GBSA binding energy calculation details

The binding energies between DNA and protein were calculated with 1000 snapshots extracted from MD trajectories by molecular mechanics/generalized Born surface area (MM/GBSA) approach for binding energy-residue decomposition analysis. The MM/GBSA calculations were performed under the condition of IGB=2 and ionic strength of 100 mM, as in the previous literature (*Proteins: Struct., Funct., Genet.* 2004, 55, 383-394). The surface tension constants γ and β were set to 0.0072 and 0 in the nonpolar solvation free energy, respectively. Typically, 1000 snapshots were extracted from the equilibrium trajectories (100 ns) for binding free energy calculations using *mm_mpsa.py* as follows: $\Delta G_{\text{MM/GBSA}} = \Delta E_{\text{vdW}} + \Delta E_{\text{ele}} + \Delta G_{\text{pol}} + \Delta G_{\text{nonpol}}$. In the per-residue energy decomposition analysis, the contribution of each residue was estimated with *idecomp* = 2, by which the 1-4 EEL interaction energies were added to the electrostatic potential term and the 1-4 VDW interaction energies to the van der Waals potential term.

Non-covalent interaction analysis details

The IGM analysis depends on the topological characteristics of the electron density, ρ . The IGM descriptor δg^{inter} is given by the difference between the first derivatives of the charge densities for the total system and the fragments:

$$\delta g(r)^{\text{inter}} = |\nabla \rho^{\text{IGM,inter}}| - |\nabla \rho|$$

$\delta g^{\text{inter}} > 0$ indicates the presence of weak interactions, and the magnitude of the descriptor at a point in space indicates the strength of the interaction.

The non-covalent interaction RDG method is an alternative method to reveal weak interlayer interactions (4), with a dimensionless form of electron density gradient norm function:

$$\text{RDG}(r) = \frac{1}{2(3\pi^2)^{1/3}} \frac{|\nabla \rho(r)|}{\rho(r)^{4/3}}$$

The sign of the second eigenvalue of the electron density Hessian matrix, $\text{sign}(\lambda_2)$, was used in the RDG analyses to judge the attractive and repulsive interaction, that is, corresponding to negative and positive values of $\text{sign}(\lambda_2) \rho$, respectively.

Furthermore, atoms in molecules (AIM) analysis (5,6) are employed to visualize the strength of intramolecular interaction. In AIM analysis, the points at where the gradient norm of function value is zero (except at infinity) were called critical points (CPs). The appearance of a (3, -1) type of critical point usually appeared on a bond path or between the atoms which had attractive interaction, hence called a bond critical point (BCP). According to the AIM theory, the ρ and its Laplacian value ($\nabla^2 \rho$) were used to indicate strength and nature, respectively. Recently, an empirical formula to estimate binding energy has been proposed by Emamian, Lu, and co-workers (7). According to their method, the electron density at the bond critical point (ρ_{BCP}) shows a linear dependence on the binding energy (BE): namely, $\text{BE (kcal/mol)} = -223.08 \times \rho_{\text{BCP (au)}} + 0.7423$ or $-332.34 \times \rho_{\text{BCP (au)}} - 1.0661$ for neutral complexes and charged complexes, respectively.

References

(1) Yu, H., Li, J., Liu, G., Zhao, G., Wang, Y., Hu, W., et al. (2020). DNA backbone interactions impact the sequence specificity of DNA sulfur-binding domains: revelations from structural

analyses. *Nucleic Acids Res.* **15** 8755-8766.

2. Shirts, M. R.; Chodera, J. D. Statistically optimal analysis of samples from multiple equilibrium states. *J. Chem. Phys.* 2008, **129** (12), 124105
3. Lefebvre, C., Rubez, G., Khartabil, H., Boisson, J.C., Contreras-Garcia, J. and Henon, E. (2017) Accurately extracting the signature of intermolecular interactions present in the NCI plot of the reduced density gradient versus electron density. *Phys. Chem. Chem. Phys.*, **19**, 17928–17936.
4. Johnson, E.R., Keinan, S., Mori-Sanchez, P., Contreras-Garcia, J., Cohen, A.J. and Yang, W. (2010) Revealing non-covalent interactions. *J. Am. Chem. Soc.*, **132**, 6498-6506.
5. Fuster, F., and Silvi, B. (2000). Does the topological approach characterize the hydrogen bond? *Theor. Chem. Acc.* **104**, 13-21
6. Bader, R. W. F. *Atoms in Molecules. A Quantum Theory*; International Monographs on Chemistry; Clarendon Press: Oxford, 1990; Vol. 22, pp 1-438.
7. Emamian, S.; Lu, T.; Kruse, H.; Emamian, H. Exploring Nature and Predicting Strength of Hydrogen Bonds: A Correlation Analysis Between Atoms-in-Molecules Descriptors, Binding Energies, and Energy Components of Symmetry-Adapted Perturbation Theory. *J. Comput. Chem.* 2019, **40**, 2868-2881

Geometries of the complexes discussed in the paper

1. PS-P165 complex in chalcogen bond analyses.

Center Number	Atomic Number	Atomic Type	Coordinates (Angstroms)		
			X	Y	Z
1	6	0	-2.415024	1.447506	-0.461135
2	8	0	-2.469411	1.751222	-1.632307
3	7	0	-2.682948	0.205731	-0.021597
4	6	0	-2.197082	2.564647	0.576220
5	6	0	-2.915839	-0.911486	-1.003720
6	6	0	-2.570415	-0.291186	1.360894
7	1	0	-1.312462	2.365466	1.193011
8	1	0	-2.055436	3.493143	0.023216
9	1	0	-3.062507	2.659193	1.244991
10	6	0	-2.818367	-2.185938	-0.149425
11	1	0	-2.159502	-0.853725	-1.789376
12	1	0	-3.905121	-0.779918	-1.461719
13	6	0	-3.164476	-1.702381	1.233508
14	1	0	-3.129381	0.339289	2.061957
15	1	0	-1.514252	-0.322832	1.661515
16	1	0	-1.785256	-2.550216	-0.178297
17	1	0	-3.479478	-2.982168	-0.507309
18	1	0	-2.801825	-2.365777	2.027796
19	1	0	-4.257036	-1.636263	1.345590
20	16	0	0.763901	-0.328540	-0.506836
21	15	0	2.790731	-0.348951	-0.346745
22	8	0	3.476533	0.953272	-1.030772
23	8	0	3.247992	-0.193423	1.176432
24	8	0	3.517790	-1.578785	-0.825360
25	1	0	2.793252	1.415138	-1.543459
26	6	0	2.881292	0.937720	1.988747
27	1	0	3.310537	1.863496	1.582320
28	1	0	1.788488	1.037777	2.036395
29	1	0	3.283473	0.756602	2.990623

2. P165 in PS-P165 complex

Center Number	Atomic Number	Atomic Type	Coordinates (Angstroms)		
			X	Y	Z
1	6	0	-2.415024	1.447506	-0.461135
2	8	0	-2.469411	1.751222	-1.632307
3	7	0	-2.682948	0.205731	-0.021597
4	6	0	-2.197082	2.564647	0.576220
5	6	0	-2.915839	-0.911486	-1.003720
6	6	0	-2.570415	-0.291186	1.360894
7	1	0	-1.312462	2.365466	1.193011
8	1	0	-2.055436	3.493143	0.023216
9	1	0	-3.062507	2.659193	1.244991
10	6	0	-2.818367	-2.185938	-0.149425
11	1	0	-2.159502	-0.853725	-1.789376
12	1	0	-3.905121	-0.779918	-1.461719
13	6	0	-3.164476	-1.702381	1.233508
14	1	0	-3.129381	0.339289	2.061957
15	1	0	-1.514252	-0.322832	1.661515
16	1	0	-1.785256	-2.550216	-0.178297
17	1	0	-3.479478	-2.982168	-0.507309
18	1	0	-2.801825	-2.365777	2.027796
19	1	0	-4.257036	-1.636263	1.345590

3. PS in PS-P165 complex

Center Number	Atomic Number	Atomic Type	Coordinates (Angstroms)		
			X	Y	Z
1	6	0	-2.415024	1.447506	-0.461135
2	8	0	-2.469411	1.751222	-1.632307
3	7	0	-2.682948	0.205731	-0.021597
4	6	0	-2.197082	2.564647	0.576220
5	6	0	-2.915839	-0.911486	-1.003720
6	6	0	-2.570415	-0.291186	1.360894
7	1	0	-1.312462	2.365466	1.193011
8	1	0	-2.055436	3.493143	0.023216
9	1	0	-3.062507	2.659193	1.244991
10	6	0	-2.818367	-2.185938	-0.149425
11	1	0	-2.159502	-0.853725	-1.789376
12	1	0	-3.905121	-0.779918	-1.461719
13	6	0	-3.164476	-1.702381	1.233508
14	1	0	-3.129381	0.339289	2.061957
15	1	0	-1.514252	-0.322832	1.661515
16	1	0	-1.785256	-2.550216	-0.178297
17	1	0	-3.479478	-2.982168	-0.507309
18	1	0	-2.801825	-2.365777	2.027796
19	1	0	-4.257036	-1.636263	1.345590

Number	Number	Type	X	Y	Z
1	16	0	0.763901	-0.328540	-0.506836
2	15	0	2.790731	-0.348951	-0.346745
3	8	0	3.476533	0.953272	-1.030772
4	8	0	3.247992	-0.193423	1.176432
5	8	0	3.517790	-1.578785	-0.825360
6	1	0	2.793252	1.415138	-1.543459
7	6	0	2.881292	0.937720	1.988747
8	1	0	3.310537	1.863496	1.582320
9	1	0	1.788488	1.037777	2.036395
10	1	0	3.283473	0.756602	2.990623

4. NCI calculated model based on co-crystal structure

Center Number	Atomic Number	Atomic Type	Coordinates (Angstroms)		
			X	Y	Z
1	6	0	3.100203	-2.021179	1.842741
2	6	0	2.047923	-1.846383	2.931135
3	6	0	2.840603	-1.071822	0.731905
4	1	0	4.073277	-1.795111	2.279458
5	1	0	3.159475	-3.029563	1.489827
6	8	0	2.333716	-1.385420	4.033489
7	7	0	0.808646	-2.304468	2.649869
8	6	0	3.872127	-1.106625	-0.352448
9	1	0	2.867946	-0.070253	1.160422
10	1	0	1.872553	-1.313392	0.293080
11	6	0	-0.278887	-2.194533	3.616119
12	1	0	0.631157	-2.732363	1.752078
13	6	0	4.689623	-0.158075	-0.842748
14	7	0	4.095674	-2.234508	-1.116105
15	6	0	-1.656824	-2.326717	2.922378
16	1	0	-0.262592	-1.187473	4.033420
17	1	0	-0.136967	-2.815374	4.475954
18	7	0	5.418588	-0.730817	-1.863213
19	1	0	4.762226	0.873608	-0.497477
20	6	0	5.058477	-1.990147	-1.981312
21	6	0	-2.051065	-1.008795	2.266389
22	1	0	-2.405572	-2.585693	3.670772
23	1	0	-1.603368	-3.105252	2.161053
24	1	0	6.113735	-0.261335	-2.426450
25	1	0	5.485044	-2.710933	-2.678235
26	6	0	-3.394655	-1.177433	1.544498
27	1	0	-1.286359	-0.719568	1.546070
28	1	0	-2.142095	-0.236097	3.029499
29	7	0	-3.244220	-1.849806	0.274458
30	1	0	-3.802497	-0.184620	1.354076
31	1	0	-4.063604	-1.762327	2.175909
32	6	0	-4.277313	-2.410264	-0.402991
33	1	0	-2.320592	-1.905283	-0.130497
34	7	0	-4.065989	-3.033329	-1.549518
35	7	0	-5.508016	-2.400544	0.094437
36	1	0	-4.836400	-3.468369	-2.037226
37	1	0	-3.134904	-3.074146	-1.937787
38	1	0	-5.691558	-1.950960	0.979625
39	1	0	-6.261196	-2.842968	-0.412701
40	1	0	2.120148	1.723660	0.606943
41	6	0	1.970642	2.515291	1.340543
42	7	0	0.661126	3.168306	1.168552
43	6	0	1.850629	1.947297	2.763080
44	1	0	2.819704	3.184083	1.201424
45	6	0	0.265788	3.932981	0.136099
46	6	0	-0.340456	2.698113	2.189878
47	6	0	0.400957	1.591648	2.957610
48	1	0	2.492242	1.076800	2.896105
49	1	0	2.157652	2.694508	3.495561
50	6	0	1.336063	4.409762	-0.890014
51	8	0	-0.858013	4.375075	0.044060

52	1	0	-1.260970	2.344051	1.726700
53	1	0	-0.650256	3.486983	2.843029
54	1	0	0.156083	0.589725	2.604460
55	1	0	0.133746	1.602281	4.014272
56	6	0	1.807486	3.293908	-1.756332
57	1	0	0.846962	5.136435	-1.538240
58	1	0	2.150778	4.918455	-0.418450
59	1	0	0.940527	2.699393	-2.043274
60	1	0	2.526712	2.693423	-1.199338
61	1	0	2.274050	3.653082	-2.649759
62	8	0	-1.267426	-2.231720	-1.897430
63	15	0	-0.596133	-0.939411	-2.284071
64	8	0	-1.296897	-0.380035	-3.636859
65	16	0	-0.418787	0.496315	-0.855396
66	8	0	0.837880	-1.391312	-2.825110
67	6	0	-2.410843	0.511501	-3.547709
68	6	0	1.771813	-0.470979	-3.420569
69	1	0	-2.491150	0.945931	-2.550861
70	1	0	-3.282259	-0.031990	-3.847960
71	1	0	-2.279988	1.215774	-4.342554
72	1	0	1.278250	0.488024	-3.574674
73	1	0	2.627737	-0.345096	-2.757292
74	1	0	2.107386	-0.846938	-4.364468
75	1	0	-2.797777	2.706491	0.120092
76	6	0	-3.794269	2.863729	-0.292344
77	6	0	-4.509180	3.896709	0.515543
78	1	0	-4.352018	1.927238	-0.261279
79	1	0	-3.710579	3.203059	-1.324851
80	1	0	-5.227221	4.433733	-0.104645
81	1	0	-3.840796	4.656899	0.862349
82	1	0	-5.061862	3.407132	1.289983

5. PS-H₂O model

Center Number	Atomic Number	Atomic Type	Coordinates (Angstroms)		
			X	Y	Z
1	8	0	1.518567	0.272781	-0.657230
2	15	0	-0.04521	0.284079	-0.282905
3	8	0	-0.743087	0.930931	-1.449256
4	16	0	-0.37858	1.038930	1.521382
5	8	0	-0.309956	-1.312530	-0.289144
6	8	0	-2.575246	2.716940	-0.410581
7	1	0	-2.254822	2.554704	0.490571
8	1	0	-1.984024	2.121158	-0.921223
9	6	0	-1.612283	-1.834468	0.053265
10	1	0	-1.909239	-1.422622	1.019604
11	1	0	-2.331514	-1.504932	-0.699880
12	6	0	-1.524292	-3.339671	0.104039
13	1	0	-2.500102	-3.754065	0.364393
14	1	0	-1.224829	-3.747898	-0.862813
15	1	0	-0.8027	-3.659733	0.857782
16	6	0	2.499427	-0.351200	0.204307
17	1	0	2.229005	-0.156306	1.243419
18	1	0	2.468346	-1.428339	0.031376
19	6	0	3.85635	0.220088	-0.123307
20	1	0	4.613876	-0.256051	0.502274
21	1	0	4.113852	0.041669	-1.168841
22	1	0	3.880151	1.294879	0.064648

6. PO-H₂O model

Center Number	Atomic Number	Atomic Type	Coordinates (Angstroms)		
			X	Y	Z
1	8	0	1.356692	0.036882	-0.355350
2	15	0	-0.048784	-0.431730	0.338215
3	8	0	0.084729	-0.404804	1.844794
4	8	0	-1.016615	0.757839	-0.201923
5	8	0	-3.191822	-2.334417	-0.480009
6	1	0	-2.236318	-2.100883	-0.421440

7	1	0	-3.275545	-2.822451	-1.307250
8	6	0	-0.862940	2.108985	0.315815
9	1	0	-1.144796	2.109684	1.371028
10	1	0	0.186895	2.401046	0.232906
11	6	0	-1.750293	3.026067	-0.493156
12	1	0	-2.797286	2.722057	-0.418311
13	1	0	-1.661255	4.047297	-0.112784
14	1	0	-1.456963	3.023446	-1.545792
15	6	0	2.615161	-0.498446	0.132592
16	1	0	2.769679	-0.147999	1.155732
17	1	0	2.562344	-1.590883	0.141018
18	6	0	3.715180	-0.018061	-0.785679
19	1	0	3.757178	1.073969	-0.803601
20	1	0	4.678806	-0.392845	-0.430030
21	1	0	3.559593	-0.382293	-1.804145
22	8	0	-0.547138	-1.702434	-0.326011

7. PO-P165 complex calculated in the orbital interaction diagram

Center Number	Atomic Number	Atomic Type	Coordinates (Angstroms)		
			X	Y	Z
1	6	0	-2.415024	1.447506	-0.461135
2	8	0	-2.469411	1.751222	-1.632307
3	7	0	-2.682948	0.205731	-0.021597
4	6	0	-2.197082	2.564647	0.576220
5	6	0	-2.915839	-0.911486	-1.003720
6	6	0	-2.570415	-0.291186	1.360894
7	1	0	-1.312462	2.365466	1.193011
8	1	0	-2.055436	3.493143	0.023216
9	1	0	-3.062507	2.659193	1.244991
10	6	0	-2.818367	-2.185938	-0.149425
11	1	0	-2.159502	-0.853725	-1.789376
12	1	0	-3.905121	-0.779918	-1.461719
13	6	0	-3.164476	-1.702381	1.233508
14	1	0	-3.129381	0.339289	2.061957
15	1	0	-1.514252	-0.322832	1.661515
16	1	0	-1.785256	-2.550216	-0.178297
17	1	0	-3.479478	-2.982168	-0.507309
18	1	0	-2.801825	-2.365777	2.027796
19	1	0	-4.257036	-1.636263	1.345590
20	15	0	2.790731	-0.348951	-0.346745
21	8	0	3.476533	0.953272	-1.030772
22	8	0	3.247992	-0.193423	1.176432
23	8	0	3.517790	-1.578785	-0.825360
24	1	0	2.793252	1.415138	-1.543459
25	6	0	2.881292	0.937720	1.988747
26	1	0	3.310537	1.863496	1.582320
27	1	0	1.788488	1.037777	2.036395
28	1	0	3.283473	0.756602	2.990623
29	8	0	1.086127	-0.331785	-0.481385

8.P165 in PO-P165 complex

Center Number	Atomic Number	Atomic Type	Coordinates (Angstroms)		
			X	Y	Z
1	6	0	-2.415024	1.447506	-0.461135
2	8	0	-2.469411	1.751222	-1.632307
3	7	0	-2.682948	0.205731	-0.021597
4	6	0	-2.197082	2.564647	0.576220
5	6	0	-2.915839	-0.911486	-1.003720
6	6	0	-2.570415	-0.291186	1.360894
7	1	0	-1.312462	2.365466	1.193011
8	1	0	-2.055436	3.493143	0.023216
9	1	0	-3.062507	2.659193	1.244991
10	6	0	-2.818367	-2.185938	-0.149425
11	1	0	-2.159502	-0.853725	-1.789376
12	1	0	-3.905121	-0.779918	-1.461719
13	6	0	-3.164476	-1.702381	1.233508
14	1	0	-3.129381	0.339289	2.061957
15	1	0	-1.514252	-0.322832	1.661515

16	1	0	-1.785256	-2.550216	-0.178297
17	1	0	-3.479478	-2.982168	-0.507309
18	1	0	-2.801825	-2.365777	2.027796
19	1	0	-4.257036	-1.636263	1.345590

8. PO in PO-P165 complex

Center Number	Atomic Number	Atomic Type	Coordinates (Angstroms)		
			X	Y	Z
1	15	0	2.790731	-0.348951	-0.346745
2	8	0	3.476533	0.953272	-1.030772
3	8	0	3.247992	-0.193423	1.176432
4	8	0	3.517790	-1.578785	-0.825360
5	1	0	2.793252	1.415138	-1.543459
6	6	0	2.881292	0.937720	1.988747
7	1	0	3.310537	1.863496	1.582320
8	1	0	1.788488	1.037777	2.036395
9	1	0	3.283473	0.756602	2.990623
10	8	0	1.086127	-0.331785	-0.481385
